TECHNISCHE MECHANIK, 32, 2-5, (2012), 535 – 545
submitted: November 1, 2011

Martensitic Thin Wires under Restrained Recovery: Theoretical and Experimental Aspects

R. Rizzoni, M. Merlin, V. Mazzanti

A one-dimensional model for the evolution of microstructure in single crystal shape memory wires has been recently proposed in (Rizzoni (2011)). The model is based on the constrained theory of martensite *introduced by (Ball et al. (1995); De Simone and James (2002)) and on the assumption that stable equilibrium configurations are deformations lying at the energy wells on most parts of the wire. In this paper we compare the response simulated for restrained recovery conditions (Rizzoni (2011)) with experimental data obtained in restrained recovery tests performed on NiTi wires. As an application, we consider a truss made of shape memory wires and rigid elements, and we calculate its deformation after thermal activation of the shape recovery.*

1 Introduction

Shape memory alloys (SMAs) are characterized by a reversible, diffusion-less, solid-solid phase transformation between two different crystalline phases, austenite (or parent) and martensite. At low temperatures the martensite phase is stable and the material can be deformed with strains up to 8%. Increasing the temperature causes the material to transform back into the austenite phase. During reverse transformation from martensite to austenite, the material returns to the prestrained shape. After that, if the temperature is decreased once again, the alloy goes into direct austenite to martensite transformation. In direct transformation the specimen shape remains unchanged until an external force is applied. The recovering of the original shape upon heating is known as the shape memory effect. The *restrained shape memory effect* is observed when an external constraint prevents the material from returning to the shape it had in the parent phase. For example, shape recovering induced by phase transformation is restricted in shape memory wires used for actuation purposes or for those embedded in an elastic matrix. In these situations, large recovery stresses are generated up to 700 MPa (Šittner et al. (2000); Tsoi et al. (2002, 2004b)).

Several studies have proposed constitutive phenomenological models that are able to reproduce the macroscopic response of shape memory materials in restrained recovery conditions (Brinson (1993); Kato et al. (2004); Kosel and Videnic (2007)) and in shape memory composites (Briggs and Ponte Castaneda (2002); Marfia (2005); Marfia and Sacco (2005)). Recent experimental work has shown that the evolution of the material microstructure plays an important role in the mechanism at the basis of the recovery stress generation. In particular, Zheng et al. have shown the role of the transformation of preferentially oriented martensite variants (Zheng et al. (2004)). A one-dimensional model for the evolution of the microstructure in single crystal shape memory wires has been recently proposed (Rizzoni (2011)). The model is based on the theory of thin wires developed in (Le Dret and Meunier (2003)) and on *constrained theory of martensite* introduced in (De Simone and James (2002)); the latter is based on the assumption that stable equilibrium configurations are deformations lying at the energy wells on most parts of the wire. The model is summarized in Section 2. Its input parameters are a small number of fundamental material constants: the Bain transformation matrices, describing the transformation strains from austenite to the martensite variants, and the depths of the austenite and martensite energy wells, which can be related to the latent heat of the phase transformation. On the other hand, the hysteretic behavior typical of shape memory materials cannot be captured because the equilibrium configurations are identified with the global minimizers of the energy. In (Rizzoni (2011)) the model is applied to analyze self-accommodated and detwinned microstructures and to simulate superelasticity and restrained recovery. In particular, it is shown that the model qualitatively reproduces the behavior of SMA wires in restrained recovery conditions, providing a connection between the transformation of preferentially oriented martensite variants and the experimental observation that reverse (from martensite to austenite) transformation is spread over a much wider temperature range than the transformation of a fibre in free conditions (Tsoi et al. (2004a); Zheng and Cui (2004)).

In Section 3 of this paper we compare the response of the shape memory wires under restrained recovery simulated in (Rizzoni (2011)) with the experimental data obtained in restrained recovery tests performed on NiTi wires. The percentage error between the theoretical response and the measured data is about 50%. A possible cause of the error can be attributed to the elastic deformations of the wire, which are neglected by the model proposed in (Rizzoni (2011)). Another source of error is expected to be the thermal expansion effects of the brass rods connecting the wires to the cross heads in the system used in the experiment of restrained recovery.

These results encourage the model to be applied to the analysis of smart structures. In the literature, adaptive SMA truss structures have been numerically analyzed (Bandeira et al. (2006); Toi and Tsukamoto (2011)) and their applications to hyper-redundant manipulators and shape morphing structures have been discussed (Miura et al. (1985); Sofla et al. (2009)). In Section 4 of this paper we focus on a truss made of shape memory wires and rigid elements; by selective heating of the SMA wires, it is possible to control their lengths and to create various truss shapes. We consider the simple geometry illustrate in Figure 4 and we calculate the curvature of the truss beam after thermal activation of the shape recovery. We also calculate the tip deflection and show that for the shape memory material studied in this paper, large deflections can be achieved with a reasonable number of truss units. For these reasons, this type of application is expected to offer a good potential in the design of variable geometry truss actuators.

2 Single Crystal Shape Memory Wires under Restrained Recovery Conditions

Let $\omega \subset \mathbb{R}^2$ be an open bounded domain with Lipschitz boundary and unit area and let $\omega \times (0, L)$ be the reference, undeformed configuration of the wire. We introduce a coordinate system so that the x_3-axis coincides with the undeformed axis of the wire and we denote e_3 as the x_3-axis unit vector. When the wire is very thin, Le Dret and Meunier (2003) show that its deformation is described by the deformation field $y : (0, L) \mapsto \mathbb{R}^3$ of the center line of the wire. It is shown in (Rizzoni (2011)) that, if the elastic moduli of the material are large enough, the microstructure of the material can be approximately described by a family of Young measures $x_3 \mapsto \nu_{x_3}, x_3 \in (0, L)$, supported on the set $A \cup M$, where A and M are the sets of the austenite and martensite wells, defined respectively as

$$A := SO(3) \ , \quad M =: \bigcup_{i=1}^{N} \{QU_i : Q \in SO(3)\}. \tag{1}$$

Here $SO(3)$ is the set of all proper rotations and $U_1, U_2, \ldots U_N$ denote N symmetric and positive definite 3×3 matrices describing the transformation strains from the austenite to martensite variants (Ball and James (1987, 1992); Bhattacharya (2003)). The macroscopic deformation gradient turns out to be the center of mass of the Young measure

$$y_{,3}(x_3) = \int_{A \cup M} F e_3 \, d\nu_{x_3}(F) \ , \quad \text{a.e. } x_3 \in (0, L). \tag{2}$$

Thus, a couple (ν_{x_3}, y) completely describes a configuration of the wire, in the sense that it embeds information on both the actual microstructure and on the macroscopic deformed configuration.

The stable equilibrium configurations of the wire globally minimize the free energy

$$E((\nu, y); \theta) = \mid \omega \mid \int_0^L \Big(l_m(\theta) \int_M d\nu_{x_3}(F) + l_a(\theta) \int_A d\nu_{x_3}(F) \Big) \, dx_3, \tag{3}$$

where $l_a(\theta)$, $l_m(\theta)$ are the heights of the austenite and martensite wells at temperature θ, respectively. After introducing the averaged martensite volume fraction

$$\lambda := \frac{1}{L} \int_0^L \int_M d\nu_{x_3}(F) \in [0, 1], \tag{4}$$

the energy (3) can be written in the simple form

$$E((\nu, y); \theta) = \mid \omega \mid \Big(l_m(\theta)\lambda + l_a(\theta)(1 - \lambda) \Big). \tag{5}$$

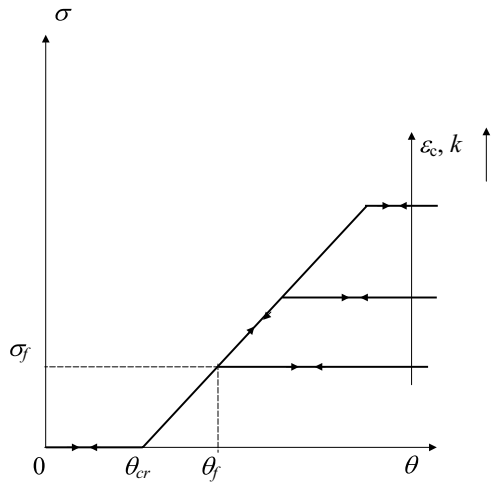

Figure 1: Simulated stress-temperature response during restrained recovery

To model the exchange of the global minimum between austenite and martensite that occurs when the temperature is changed, we take $\Delta l(\theta) := l_m(\theta) - l_a(\theta)$ to denote a monotonic increasing function in θ, and vanishing at θ_{cr}. The derivative $\Delta l'(\theta_{cr})$ can be related to the latent heat of the phase transformation in the following way

$$\Delta l(\theta) \approx \frac{q\rho}{\theta_{cr}}(\theta - \theta_{cr}), \tag{6}$$

where ρ is the density of the material and q is the latent heat of transformation per unit mass.

To summarize, the input parameters of the model are the following material constants: the Bain transformation matrices $U_1, U_2, \ldots U_N$, of which the components can be obtained from X-ray measurements of lattice parameters of the austenite and martensite phases; the equilibrium transformation temperature θ_{cr}; and the density of the material ρ and the latent heat of transformation q. Both the transformation temperature and the latent heat can be obtained from differential scanning calorimetry measurements. Experimental data obtained in DSC tests are presented in the next section.

To study the restrained shape memory effect, Rizzoni (2011) has considered a martensitic wire with initial length L and deformed by a uniaxial extension of amount $\epsilon_c > 0$. After the deformation, the wire is bonded to a linear elastic spring of stiffness $k > 0$ and then heated above θ_{cr} while keeping the sum of the lengths of the wire and spring fixed. On heating, the material, initially made of a mixture of martensite variants, changes to a mixture of austenite and martensite, the wire partially recovers the prestrain ϵ_c, the spring deforms and stress is generated.

The theoretical stress-temperature profile is represented in Figure 1. The stress linearly increases, starting from zero at θ_{cr} and reaches a saturation level σ_f at the temperature

$$\theta_f = \theta_{cr}(1 + \frac{kL(\gamma_M - 1)}{q\rho}\epsilon_c) \ , \tag{7}$$

where $\gamma_M := \max\{|\ U_i e_3\ |\ :\ i = 1, 2, \ldots N\}$ is the maximum elongation achievable during the phase transformation. As illustrated in Figure 1, the saturation stress

$$\sigma_f := \frac{q\rho}{\theta_{cr}}\frac{(\theta_f - \theta_{cr})}{(\gamma_M - 1)} \tag{8}$$

increases with both prestrain and spring stiffness. These results are in qualitative agreement with some thermomechanical characteristics of shape memory alloys observed in experiments of restrained recovery; in particular, the maximum recovery stress was found to increase with increasing prestrain and the increase of constraining stress produces a shift in the transformation temperatures to higher temperatures (Šittner et al. (2000); Vokoun

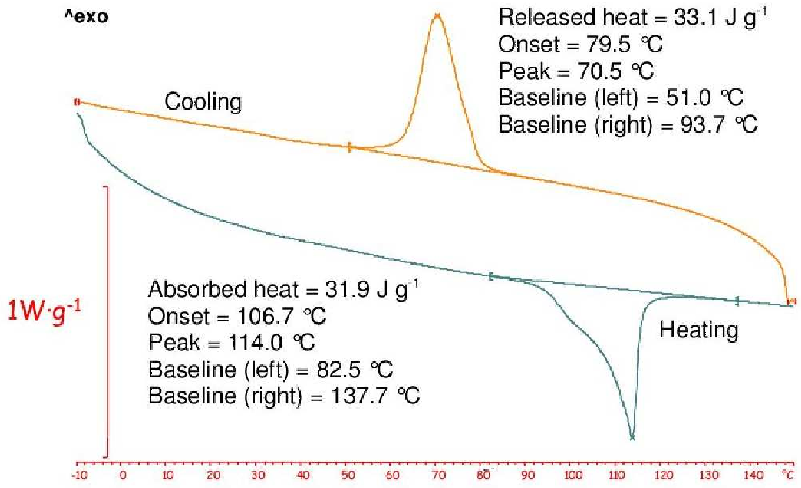

Figure 2: DSC heating (lower) and cooling (upper) curves.

et al. (2003)). Further qualitative comparison of the results of the model with other experimental findings can be found in (Rizzoni (2011)). In the next section, we compare the theoretical stress-temperature profile given by (8) with the first heating cycle obtained in a test of restrained recovery.

3 Material Characterization, Instrument and Test Methodology

A commercial NiTi wire provided by SAES Getters S.p.A. (Italy), with a normal composition of 50.5 at.% Ni was investigated. The wire was martensitic and polycrystalline at room temperature with a nominal diameter of 0.48 mm. The wire was tested without any further surface treatment or modifications.

A Differential Scanning Calorimetry (DSC) test was carried out on small fractions of the wire. The DSC samples had a weight of 12 mg and we used a constant heating/cooling rate of 10 °C/min. Figure 2 shows the DSC thermogram. According to literature the characteristic martensitic and austenitic starting and finishing temperatures, M_s, M_f, A_s, and A_f, were determined by the intersection between the baseline of the DSC curves and the tangents to the peaks. Table 1 presents the results and the latent heats per unit mass of the alloy in the range of the phase changes on heating and cooling. The mean of the characteristic temperatures, 88.5°C, is assumed to provide an estimate for θ_{cr}.

Free recovery tests were performed on samples with two different lengths (150 mm and 115 mm) to determine the prestrain ϵ_c, not specified by the manufacturer. After heating up to 200°C and cooling down to room temperature, the final lengths of the wires were measured. A prestrain of 5.5% was estimated for both sets.

To evaluate the maximum recoverable strain ϵ_L, uniaxial tensile tests were performed at 25°C on 100 mm long wires. An Instron 4467 testing machine with a 500 N load cell was used and all tests were performed under displacement controlled loading conditions and at the relatively low loading rate of 1 mm/min. The maximum strain achievable during the phase transformation was of 6% Merlin (2008). This value is assumed to provide a reasonable estimate for γ_M.

Experiments of restrained recovery were carried out heating a 120 mm long wire from 25°C to 150°C under zero displacement conditions. The Instrom 4467 and a convective air thermal bath (Criotest - Mazzali system) were used. The temperature was measured with a thermocouple placed close to the wire. The rate of heating

Table 1: Transformation temperatures and latent heats per unit mass of the reverse ($M \to A$) and direct ($A \to M$) phase transformation as determined by DSC.

A_s [°C]	A_f [°C]	$\Delta H_{M\to A}$ [J g^{-1}]	M_s [°C]	M_f [°C]	$\Delta H_{A\to M}$ [J g^{-1}]
92	118	31.9	82	62	33.1

was 4°C/min. This rate was chosen because it produces a smooth and slow temperature trend during heating and cooling, which allows a pseudo-steady state to be maintained inside the wire. The stress-temperature profiles of two first heating cycles are presented in Figure 3. Linear interpolation of the two profiles between the temperatures 80°C and 150°C provides slopes of 6.9 MPa °C^{-1} and 6.1 MPa °C^{-1} and horizontal intercepts of 81.0 °C and 87.0 °C.

Substituting the values $q = \Delta H_{M\to A} = 31.9$ J g^{-1}, $\theta_{cr} = 82.5$ °C, $\gamma_M = 0.06$, and assuming a density of $\rho = 6.45$ g cm^{-3}, relations (7) and (8) provide a stress rate of 9.64 MPa °C^{-1}. The percentage error between this theoretical value and the mean of the measured values is about 50%. A possible explanation of the error is that the model used to obtain relation (7) neglects the elastic deformations of the wire, which are expected to reduce the stress rate. Another source of error is expected to be the thermal expansion effects of the brass rods connecting the wires to the cross heads in the Criotest - Mazzali system. Finally, it should be noted that relations (7) and (8) provide for the stress rate $d\sigma/d\theta$ a relation which coincides with the Clausius-Clapeyron equation. This equation is known to be appropriate to single crystals and to a single variant transformation. In polycrystalline materials, $d\sigma/d\theta$ is found to depend on temperature and to increase with increasing prestrain (Tsoi et al. (2004a); Šittner et al. (2000); Vokoun et al. (2003)).

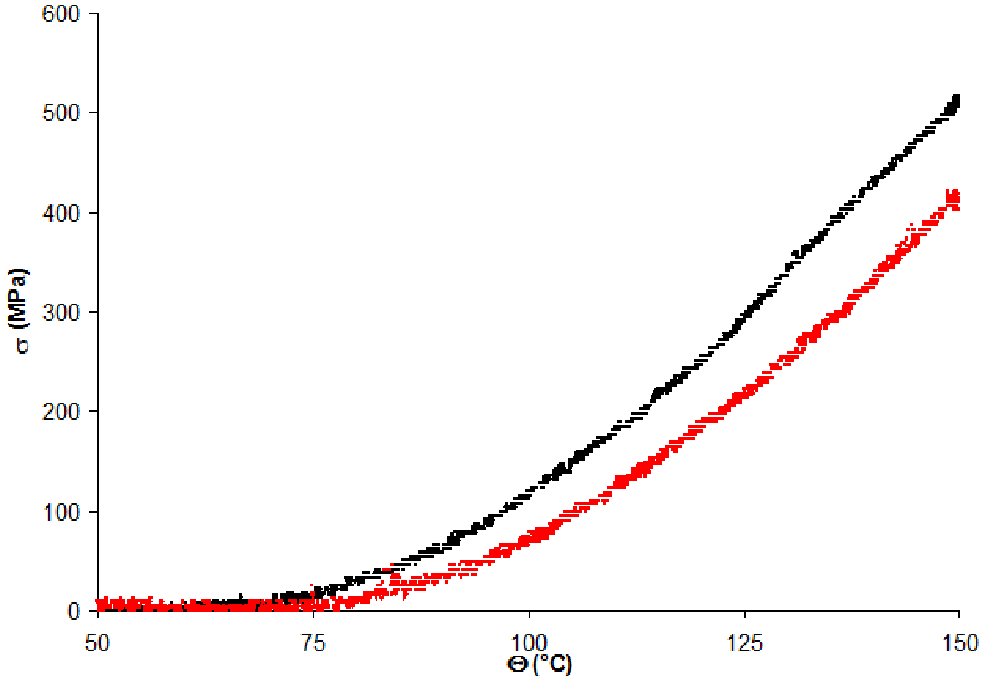

Figure 3: Stress-temperature profiles of two first heating cycles in restrained recovery conditions.

4 A Variable Geometry Truss

In this section we study the planar truss composed of SMA wires and rigid members as represented in Figure 4. Before being connected to the rigid elements, the SMA wires first had a length L in the austenitic phase, they were then cooled below the transformation temperature and, finally, they underwent elongation imposing them on a recoverable axial strain $\epsilon_c \in (0, \gamma_M - 1]$. By heating the SMA wires, it is possible to vary their lengths and create various truss shapes. Here we consider the case when all the SMA wires depicted in red are simultaneously activated, i.e. simultaneously heated above the transformation temperature. In absence of external loads and under the assumption that each unit undergoes the same deformation, the structure takes the form of a circular arch whose radius is known if the deformations of the activated and unactivated SMA wires are known. In the model recalled in section 2, the deformation of an SMA wire is related to the average martensite volume fraction via the Young measure (cfr. (2)) and the relevant parameter is the average martensite volume fraction (cfr. (4)). Moreover, if m is taken to denote the number of units, the equilibrium configuration of the structure minimises the total energy

$$E((\nu, y); \theta) = m \mid \omega \mid L(\Delta l(\theta_1)\lambda_1 + \Delta l(\theta_2)\lambda_2 + 2l_a) \tag{9}$$

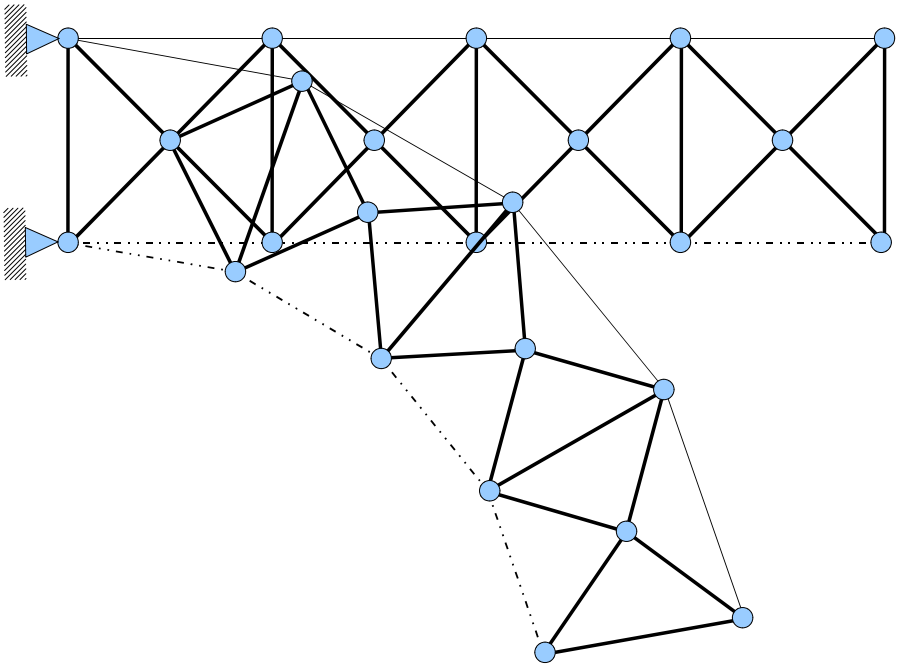

Figure 4: Initial and deformed configurations of a planar variable geometry truss built with rigid members (bold lines) and SMA wires (activated wires are presented as dotted lines, unactivated wires are presented as thin solid lines).

where $\theta_1 > \theta_c$ and $\lambda_1 \in [0,1]$ are the temperature and average martensite volume fraction in each activated SMA wire, and $\theta_2 < \theta_c$ and $\lambda_2 \in [0,1]$ are the temperature and average martensite volume fraction in each unactivated SMA wire. As $\Delta l(\theta_1) > 0$ and $\Delta l(\theta_2) < 0$, a lower bound for the energy (9) is attained at $\lambda_2 = 1$, meaning that it is energetically more convenient for the unactivated SMA wires to remain in the martensitic state. On the other hand, the unactivated wires have to lengthen in order to allow prestrain recovery in the activated wires. In other words, the unactivated wires undergo detwinning. In Rizzoni (2011), detwinning is analyzed by introducing the average volume fractions of the martensite variants:

$$\eta_i := \frac{1}{L}\int_0^L \int_{SO(3)U_i} d\nu_{x_3}(F) \in [0,1], \quad i = 1, 2, \dots N, \tag{10}$$

with

$$\sum_{i=1}^{N} \eta_i = \lambda_2 = 1. \tag{11}$$

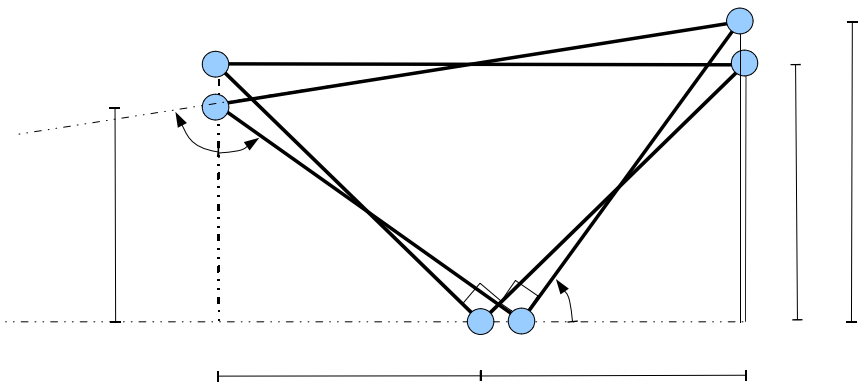

Figure 5: Analysis of the truss unit.

It should be noted that, in view of (2), the deformation of the unactivated SMA wires is given by

$$y_{,3}(x_3) = (\sum_{i=1}^{N} \gamma_i \eta_i) e_3 \quad \text{a.e. } x_3 \in (0, L), \tag{12}$$

where $\gamma_i := \mid U_i e_3 \mid$ is the axial strain corresponding to the i-th martensite variant and it should also be noted that the deformation of the unactivated bar, referred to the austenitic state here taken as reference configuration, is also given by $l_2 L^{-1}$, where l_2 is taken to denote the length of the unactivated SMA wires after heating (Figure 5). From (12) we obtain

$$\sum_{i=1}^{N} \gamma_i \eta_i = \frac{l_2}{L}. \tag{13}$$

As $\eta_i \in [0, 1]$ and $\gamma_i > 0$, the latter relation imposes the following restriction on the length l_2

$$L\gamma_m \leq l_2 \leq L\gamma_M, \tag{14}$$

where $\gamma_m := \min\{\mid U_i e_3 \mid : i = 1, 2, \dots N\}$ is the minimum strain achievable in the martensitic state. The lengths l_1 and l_2 and the hinge angle θ are related by the following geometric constraint:

$$l_1 = l\sqrt{2}\cos\theta, \tag{15}$$
$$l_2 = l\sqrt{2}\sin\theta. \tag{16}$$

Finally, condition (2) imposes the following restriction on the length l_1 :

$$l_1 = L((\gamma_M - 1)\lambda_1 + 1). \tag{17}$$

To summarize, a lower bound for the total energy (9) can be found by minimizing the quantity:

$$m \mid \omega \mid L\Big(\frac{\Delta l(\theta_1)}{(\gamma_M - 1)}(\sqrt{2}(1+\epsilon_c)\cos\theta - 1) + \Delta l(\theta_2) + 2l_a\Big) \to \min \tag{18}$$

under the constraints:

$$\frac{\sqrt{2}}{2(1+\epsilon_c)}\gamma_m \leq \sin\theta \leq \frac{\sqrt{2}}{2(1+\epsilon_c)}\gamma_M, \tag{19}$$
$$\frac{\sqrt{2}}{2(1+\epsilon_c)} \leq \cos\theta \leq \frac{\sqrt{2}}{2(1+\epsilon_c)}\gamma_M. \tag{20}$$

This minimization problem is equivalent to minimizing (18) under the condition

$$\max\{\arcsin\Big(\frac{\sqrt{2}\gamma_m}{2(1+\epsilon_c)}\Big), \arccos\Big(\frac{\sqrt{2}\gamma_M}{2(1+\epsilon_c)}\Big)\} \leq \theta \leq \min\{\arcsin\Big(\frac{\sqrt{2}\gamma_M}{2(1+\epsilon_c)}\Big), \arccos\Big(\frac{\sqrt{2}}{2(1+\epsilon_c)}\Big)\}. \tag{21}$$

As $\Delta l(\theta_1) > 0$, the minimum is attained at

$$\theta_{min} = \min\{\arcsin\Big(\frac{\sqrt{2}\gamma_M}{2(1+\epsilon_c)}\Big), \arccos\Big(\frac{\sqrt{2}}{2(1+\epsilon_c)}\Big)\}, \tag{22}$$

and two cases arise, depending upon the value of the prestrain ϵ_c. Let us put $\epsilon_c^* := \frac{\sqrt{2}}{2}\sqrt{\gamma_M^2 + 1} - 1$.

- If $0 \leq \epsilon_c \leq \epsilon_c^*$, then $\theta_{min} = \arccos\Big(\frac{\sqrt{2}}{2(1+\epsilon_c)}\Big)$. Correspondingly, we have $l_{1,min} = L$, meaning that the activated wire fully recovers its prestrain. Moreover,

$$l_{2,min} = L\sqrt{2}(1+\epsilon_c)\sqrt{1 - \frac{1}{2(1+\epsilon_c)^2}}, \tag{23}$$

which means that the unactivated wire lengthens via detwinning, as it can be easily proved that $l \leq l_2 \leq L\gamma_M$.

- If $\epsilon_c^* < \epsilon_c \leq \gamma_M - 1$, then $\theta_{min} = \arcsin\left(\frac{\sqrt{2}\gamma_M}{2(1+\epsilon_c)}\right)$. Correspondingly, we have $l_{2,min} = L\gamma_M$, meaning that the unactivated wire attains the maximum length achievable by detwinning. We also obtain

$$l_{1,min} = L\sqrt{2}(1+\epsilon_c)\sqrt{1 - \frac{\gamma_M}{2(1+\epsilon_c)^2}}. \tag{24}$$

It can be easily proved that $l_{1,min} > L$; thus, the activated wire is prevented from fully recovering its prestrain.

These results provide a lower bound for the energy (9). Using constructions presented in (Rizzoni, 2011, sects. 3, 5), it is possible to show that there is a sequence of deformations for the activated wire and a sequence for the unactivated wire achieving the energy lower bound. Note also that, if the temperature $\theta_2 < \theta_{cr}$ is kept fixed and θ_1 is slowly increased starting from a value less than θ_{cr}, the minimizing solution applies as soon as $\theta_1 > \theta_{cr}$, indicating that the truss is predicted to deform suddenly at the temperature θ_{cr}. This is consistent with the fact that the model neglects hysteresis.

Simple geometric considerations provide the curvature radius of the truss beam. This is given by

$$R = L\cot\Big(\arccos\Big(\frac{\sqrt{2}}{2(1+\epsilon_c)}\Big) - \frac{\pi}{4}\Big) + \frac{\sqrt{2}L(1+\epsilon_c)}{2}\Big(\frac{\sqrt{2}}{2(1+\epsilon_c)} + \sqrt{1 - \frac{1}{2(1+\epsilon_c)^2}}\Big), \tag{25}$$

if $0 \leq \epsilon_c \leq \epsilon_c^*$, and by

$$R = L(1+\epsilon_c)\sqrt{2}\sqrt{1 - \frac{\gamma_M^2}{2(1+\epsilon_c)^2}}\cot\Big(\arcsin\Big(\frac{\sqrt{2}\gamma_M}{2(1+\epsilon_c)}\Big) - \frac{\pi}{4}\Big) + \frac{\sqrt{2}L(1+\epsilon_c)}{2}\Big(\frac{\sqrt{2}\gamma_M}{2(1+\epsilon_c)} + \sqrt{1 - \frac{\gamma_M^2}{2(1+\epsilon_c)^2}}\Big) \tag{26}$$

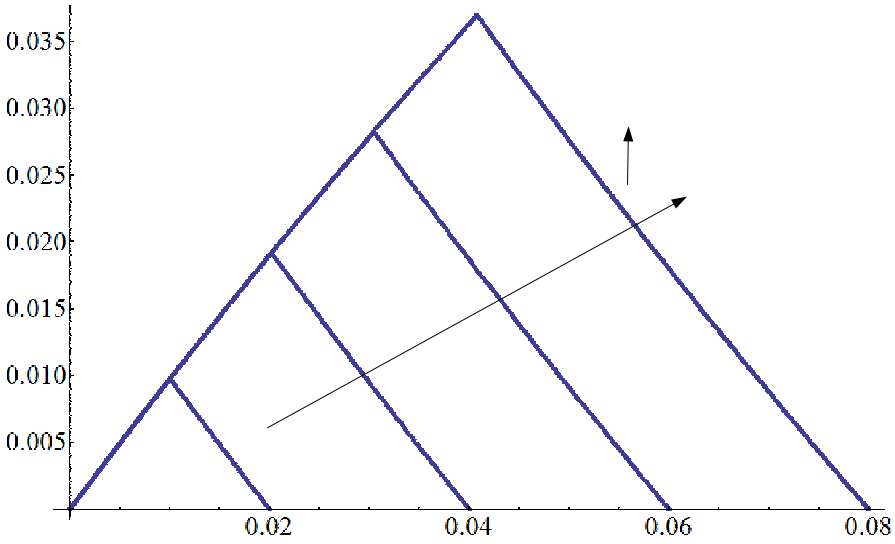

Figure 6: Truss curvature variation as a function of the prestrain ϵ_c. The following increasing values of the transformation strain, γ_M, are considered: $\gamma_M = 1.02, 1.04, 1.06, 1.08$.

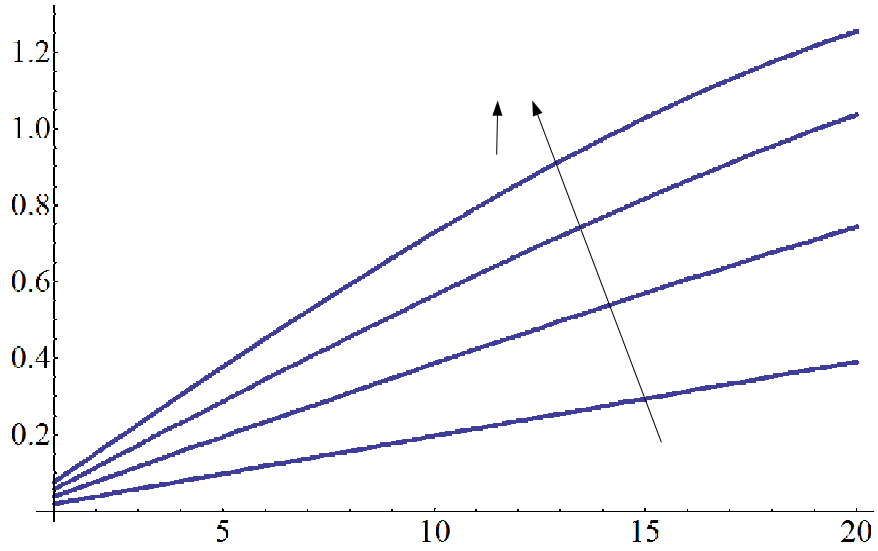

Figure 7: Tip deflection of the truss beam as a function of the number of units, m. The same increasing values of the transformation strain adopted in Figure 6 are considered.

if $\epsilon_c^* < \epsilon_c \leq \gamma_M - 1$. Figure 6 illustrates the variation of the ratio L/R as a function of the prestrain ϵ_c for different values of γ_M. The plot shows that the curvature attains the maximum value

$$\frac{2}{L}\Big(1+\gamma_M^2-2\tan\Big(\frac{\pi}{4}+\arcsin\Big(\frac{\gamma_M}{\sqrt{1+\gamma_M^2}}\Big)\Big)\Big)^{-1} \tag{27}$$

at the prestrain ϵ_c^*.

To complete the analysis of the truss unit, we note that the tip deflection, δ, of the beam truss after activation can be expressed as

$$\delta = R\Big(1-\cos(m\frac{\pi}{2}-2m\theta)\Big). \tag{28}$$

Figure 7 shows the variation of the tip deflection per unit length, $\delta/(ml)$ of the truss beam as a function of the number of truss units in the case where the maximum curvature is attained (i.e. for $\epsilon_c = \epsilon_c^*$). Table 2 collects the calculated values of the ratio $\delta/(ml)$ for several values of the number of units m in the case $\gamma_M = 1.06$, which is assumed to apply for the SMA wires studied in section 3. A tip deflection approximately equal to the 40% of the truss length was experimentally obtained on NiTi strips trained to memorize the shape of a circular arch (Merlin and Rizzoni (2011)). The same deflection is expected to be obtained in a truss actuator having 7 units.

Table 2: Theoretical values of the tip deflection per unit length, $\delta/(ml)$, for several values of the number of units m. The table refers to the case $\gamma_M = 1.06$.

m	$\delta/(ml)$
1	0.058
3	0.174
5	0.289
7	0.402
10	0.566
15	0.819
20	1.038

5 Conclusion and Perspectives

The main objective of this paper was to validate the one-dimensional model proposed in (Rizzoni (2011)) by means of experiments of restrained recovery on NiTi wires. The theoretical response obtained for restrained recovery was found to present an error of 50% when compared with the experimental data of the first heating cycle. We attributed the error to different possible causes: the thermal expansion of the system used in the experiments of restrained recovery, the effect of the elastic strains and the polycrystallinity of the material.

As a second objective, we applied the model to simulate the behavior of a variable geometry truss incorporating SMA elements. For the simple geometry illustrated in figure 4, we calculated the curvature of the truss beam and the tip deflection after thermal activation of the shape recovery. We showed that the maximum curvature can be achieved for an optimal value of the prestrain of the SMA wires. We also obtained that, for the shape memory material studied in this paper, large deflections can be achieved with a reasonable number of truss units. We note that our results are valid under the assumptions of neglecting the plastic deformations and the fighting between the grains occurring in polycrystalline SMA materials. These phenomena are known to reduce the shape memory effect, especially for large values of the prestrain. An experimental validation would then be useful to quantify the curvature reduction; in particular, to estimate the dependence of the curvature upon the prestrain several tests will be performed by means of image analysis techniques. Nevertheless, the results presented in the paper are expected to contribute to a rational design and an efficient implementation of a variable geometry truss actuator.

For adaptive structures or smart composites, performance parameters also include those associated with the matrix, such as thickness and stiffness. The interplay between these quantities and the transforming characteristics of the wires must be taken into account. For example, a minimum level of matrix stiffness is required not only to return the actuators to their original position but also to prestrain the SMA wires for the next cycle. On the other hand, excessive stiffness unavoidably reduces the deformation. To understand these issues, it would be useful to extend the analysis performed in this paper to the case of a truss actuator in contact with an elastic beam.

References

Ball, J.; Chu, C.; James, R.: Hysteresis during stress-induced variant rearrangement. *Journal de Physique IV*, 5, C8, (1995), 245–251.

Ball, J.; James, R.: Fine phase mixtures as minimizers of energy. *Archive for Rational Mechanics and Analysis*, 100, (1987), 13–52.

Ball, J.; James, R.: Proposed experimental tests of a theory of fine microstructure and the two-well problem. *Philosophical Transactions of the Royal Society of London*, A338, (1992), 389–450.

Bandeira, E.; Savi, M.; da Camara Monteiro, P.; Netto, T.: Finite element analysis of shape memory alloy adaptive trusses with geometrical nonlinearities. *Archive of Applied Mechanics*, 76, (2006), 133–144.

Bhattacharya, K.: *Microstructure of martensite. Why it forms and how it gives rise to the shape-memory effect*. Oxford University Press (2003).

Briggs, P.; Ponte Castaneda, P.: Variational estimates for the effective response of shape memory alloy actuated fibre composites. *Journal of Applied Mechanics*, 69, (2002), 470–480.

Brinson, L.: One dimensional constitutive behaviour of shape memory alloys: thermo-mechanical derivation with non-constant functions and redefined martensite internal variable. *Journal of Intelligent Material Systems and Structures*, 4, (1993), 229–242.

De Simone, A.; James, R.: A constrained theory of magnetoelasticity. *Journal of the Mechanics and Physics of Solids*, 50, (2002), 283–320.

Kato, H.; Inagaki, N.; Sasaki, K.: A one-dimensional modelling of constrained shape memory effect. *Acta Materialia*, 52, (2004), 3375–3382.

Kosel, F.; Videnic, T.: Generalized plasticity and uniaxial constrained recovery in shape memory alloys. *Mechanics of Advanced Materials and Structures*, 14, 1, (2007), 3–12.

Le Dret, H.; Meunier, N.: Heterogeneous wires made of martensitic materials. *Comptes Rendus de l'Acadmie des Sciences. Srie I. Mathmatique*, 337, (2003), 143–147.

Marfia, S.: Micro-macro analysis of shape memory alloy composites. *International Journal of Solids and Structures*, 42, (2005), 3677–3699.

Marfia, S.; Sacco, E.: Micromechanics and homogenization of sma-wire reinforced materials. *Journal of Applied Mechanics*, 72, (2005), 259–268.

Merlin, M.: Using NiTi shape memory alloy wires for the geometry active control in a cooling fan. In: *Proceedings of AGS'08 - Advances in Geomaterials and Structures*, vol. 1, Hammamet, Tunisia, May 5-7, 2008 (2008).

Merlin, M.; Rizzoni, R.: Thermoelastic transformation behavior of niti thin strips in bending: experiments and modelling. In: *CMM-2011 - Computer Methods in Mechanics*, Varsaw, Poland, May, 9-12, 2011 (2011).

Miura, K.; Furuya, H.; Suzuki, K.: Variable geometry truss and its application to deployable truss and space crane arm. *Acta Astronautica*, 12, 7/8, (1985), 599–607.

Rizzoni, R.: A constrained theory for single crystal shape memory wires with application to restrained recovery. *Continuum Mechanics and Thermodynamics*, 23, 4, (2011), 319–335.

Sofla, A.; Elzey, D.; Wadley, H.: Shape morphing hinged truss structures. *Smart Materials and Structures*, 18, 6, (2009), 065012.

Toi, Y.; Tsukamoto, K.: Computational modeling of adaptive trusses with shape memory alloy members. *Engineering Letters*, 19, 1, (2011), 31–37.

Tsoi, K. A.; Schrooten, J.; Stalmans, R.: Part i. thermomechanical characteristics of shape memory alloys. *Materials Science and Engineering A*, 368, (2004a), 286–298.

Tsoi, K. A.; Schrooten, J.; Zheng, Y.; Stalmans, R.: Part ii. thermomechanical characteristics of shape memory alloy composites. *Materials Science and Engineering A*, 368, (2004b), 299–310.

Tsoi, K. A.; Stalmans, R.; Schrooten, J.: Transformational behaviour of constrained shape memory alloys. *Acta Materialia*, 50, (2002), 3535–3544.

Šittner, P.; Vokoun, D.; Dayananda, G. N.; Stalmans, R.: Recovery stress generation in shape memory Ti_{50} Ni_{45} Cu_5. *Materials Science and Engineering A*, A286, (2000), 298–311.

Vokoun, D.; Kafka, V.; Hu, C.: Recovery stresses generated by NiTi shape memory wires under different constraint conditions. *Smart Materials and Structures*, 12, (2003), 680–685.

Zheng, Y.; Cui, L.: Martensite fraction-temperature diagram of TiNi wires embedded in an aluminum matrix. *Intermetallics*, 12, (2004), 1305–1309.

Zheng, Y.; Cui, L.; Li, Y.; Yand, D.: Separation of the martensite in TiNi fiber reinforced aluminum matrix composite. *Journal of Materials Sciences and Technology*, 20, 4, (2004), 390–394.

Address: Raffaella Rizzoni, Mattia Merlin, Valentina Mazzanti
Department of Engineering, University of Ferrara, Via Saragat 1, 44122 Ferrara.
email:raffaella.rizzoni@unife.it, mattia.merlin@unife.it, valentina.mazzanti@unife.it